Consistency of Post-Newtonian Waveforms with Numerical Relativity

John G. Baker,[1] James R. van Meter,[1,2] Sean T. McWilliams,[3] Joan Centrella,[1] and Bernard J. Kelly[1]

[1]*Gravitational Astrophysics Laboratory, NASA Goddard Space Flight Center, 8800 Greenbelt Road, Greenbelt, Maryland 20771, USA*

[2]*Center for Space Science & Technology, Physics Department, University of Maryland Baltimore County, 1000 Hilltop Circle, Baltimore, Maryland 21250, USA*

[3]*Department of Physics, University of Maryland, College Park, Maryland 20742, USA*

(Received 4 December 2006; published 29 October 2007)

General relativity predicts the gravitational wave signatures of coalescing binary black holes. Explicit waveform predictions for such systems, required for optimal analysis of observational data, have so far been achieved primarily using the post-Newtonian (PN) approximation. The quality of this treatment is unclear, however, for the important late-inspiral portion. We derive late-inspiral waveforms via a complementary approach, direct numerical simulation of Einstein's equations. We compare waveform phasing from simulations of the last ~14 cycles of gravitational radiation from equal-mass, nonspinning black holes with the corresponding 2.5PN, 3PN, and 3.5PN orbital phasing. We find phasing agreement consistent with internal error estimates for either approach, suggesting that PN waveforms for this system are effective until the last orbit prior to final merger.

DOI: 10.1103/PhysRevLett.99.181101 PACS numbers: 04.25.Dm, 04.25.Nx, 04.30.Db

Compact astrophysical binaries spiral together due to the emission of gravitational radiation. Calculating the dynamics of these systems, and the corresponding gravitational waveforms, has been a central problem in general relativity for several decades. With first-generation interferometers such as LIGO, VIRGO, and GEO600 now operating, and development moving forward on the space-based LISA mission, accurate and reliable waveforms are urgently needed for gravitational-wave data analysis.

Post-Newtonian (PN) methods, based on expansions in the parameter $\epsilon \sim v/c$, have been the major analytic tool used to calculate the system dynamics and waveforms during the early part of the inspiral, when the binary components are relatively widely separated and thus have a small orbital frequency [1]. Currently, gravitational-wave data analysis for binary inspiral relies on waveforms derived from PN methods [2]. The current predicted orbital phase is available up to $O(\epsilon^7)$, which is referred to as 3.5PN order. However, the convergence properties of the PN sequence are not well understood, and it is not yet clear how well PN predictions work late in the inspiral when frequencies are high.

Numerical relativity, in which the full set of Einstein's equations is solved on a computer, is needed to handle the final stages of the binary evolution, when the components inspiral rapidly and merge. Recently, there has been dramatic progress in the use of numerical relativity to simulate the final inspiral and merger of black holes [3–11]. These breakthroughs have allowed numerical simulations with increasingly wider initial separations, producing longer wave trains. Linking such simulations with the PN calculations and comparing their waveforms in the late-inspiral regime is a pressing concern of gravitational-wave data analysis. While qualitative comparisons have suggested that the two methods agree fairly well until shortly before the merger [7,11], our group has found that even inaccurate waveforms may approximately agree over several cycles. Quantifying the level of agreement unambiguously requires long, accurate simulations with very low eccentricity, and careful analysis.

We have carried out suitable numerical simulations of a merging equal-mass, nonspinning black-hole binary. The black holes start on nearly circular orbiting trajectories $\sim 1200M$ before merger, where M refers to the mass that the system would have had when the black holes were still far apart, before radiative losses were significant. M is related to time by $M \equiv 5 \times 10^{-6}\ \mathrm{s}(M/M_\odot)$. In this Letter, we quantitatively compare crucial phasing information in our numerical simulation waveforms with phasing in PN waveforms, finding striking agreement.

The numerical simulations were performed using the moving puncture method [4,5,12]. We use fourth-order Runge-Kutta time integration, fourth-order-accurate finite spatial differencing, and second-order-accurate initial data. Adaptive mesh refinement is used to resolve both the dynamics near the black holes and the propagation of the gravitational waves [7]. The wave extraction sphere was of radius $60M$ and the cubical outer boundary was of half-width $1536M$; more details about this simulation can be found in Ref. [13]. We performed physically equivalent runs at three different maximum resolutions: low ($3M/64$), medium ($3M/80$), and high ($M/32$). We find fourth-order convergence of the Hamiltonian constraint, and better than second-order convergence of the momentum constraints during the runs.

The simulations begin at an angular gravitational-wave frequency $\omega \sim 0.051M^{-1}$. The frequency then sweeps upward through roughly an order of magnitude while the black holes undergo ~7 orbits, producing ~14 gravitational-wave cycles before merger. For such long-lasting simulations, the primary consideration in providing a realistic initial data model is to set up the orbiting black

holes with minimal eccentricity, as gravitating binary systems of comparable-mass objects are expected to circularize rapidly through the emission of gravitational radiation. We have selected an initial black-hole configuration with the relatively low eccentricity of less than 1%, as measured below.

Figure 1 shows the gravitational-wave strain generated by our highest-resolution numerical run and that predicted by the PN approximation with 3.5PN phasing [14,15] and 2.5PN (beyond leading order) amplitude accuracy [16]. The waves are based on the dominant $l = 2$, $m = 2$ spin-weighted spherical harmonic of the radiation, and represent an observation made on the system's equatorial plane, where only one polarization component contributes to the measured strain. The initial phase and time of the waves have been adjusted so that the frequency and phase for each waveform agree at a point, $t = -1000M$, that is early in the simulation, but after transient effects from the initial data have subsided. We will quantify the phase agreement below using the frequency domain, so that the time shifting, done for illustrative purposes in Fig. 1, will have no impact on the subsequent analysis.

To conduct comparisons with PN calculations, we need to extract an instantaneous gauge-invariant polarization phase ϕ and angular frequency ω from our simulations. These are derived from the gravitational-wave strain's first time derivative, which is a robust quantity in the numerical data. This frequency corresponds to the sweep rate of the polarization angle of the circularly polarized gravitational wave that can be observed on the system's rotation axis.

We define eccentricity as a deviation from an underlying smooth, secular trend. We obtain a monotonic "secular" frequency-time relation by modeling the waveform angular frequency ω as a fourth-order monotonic polynomial

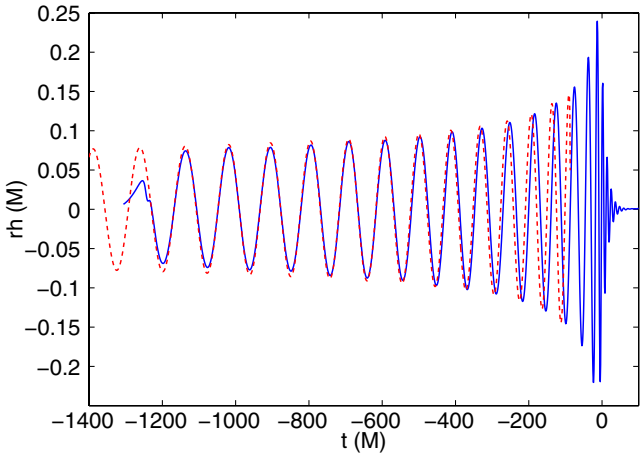

FIG. 1 (color online). Gravitational strain waveforms from the merger of equal-mass Schwarzschild black holes. The solid curve is the waveform from the high-resolution numerical simulation, and the dashed curve is a PN waveform with 3.5PN order phasing [14,15] and 2.5PN order amplitude accuracy [16]. Time $t = 0$ is the moment of peak radiation amplitude in the simulation.

$\omega_c(t)$, plus an eccentric modulation of the form $d\omega(t) = \omega(t) - \omega_c(t) = A\sin[\Phi(t)]$, where $\Phi(t)$ is a quadratic function of time. Fitting this equation to our data yields $A = 8(\pm 1) \times 10^{-4} M^{-1}$. For Keplerian systems, conserved angular momentum is proportional to $r^2\omega$, so the eccentricity corresponds to half the fractional amplitude of the frequency modulation: $e = A/(2\omega)$. In our case the eccentricity starts near 0.008, decreasing by a factor of 3 by the time $\omega_c M \sim 0.15$. We will compare our simulation with noneccentric PN calculations, with the expectation that small eccentricities have a minimal effect on the important underlying secular trend in the rate at which frequency sweeps up approaching merger.

The phasing of the waveform is critical for gravitational-wave observation. For data analysis, the optimal methods for both detection and parameter estimation rely on matched filtering, which employs a weighted inner product that can be expressed in Fourier space as $\langle h, s\rangle = \int df[\tilde{h}^*(f)\tilde{s}(f) + \tilde{h}(f)\tilde{s}^*(f)]/S_n(f)$, where h is the template being used, s is the signal being analyzed, and S_n is the one-sided power spectral density of the detector's noise [17]. A template that maximizes $\langle h, s\rangle$ will provide an optimal filter. Therefore, the most crucial factor is the relative phasing of the template and signal. The inner product will cease to accumulate in sweeping through frequency if the template and the signal evolve to be out of phase with each other by more than a half-cycle, decreasing the effectiveness of the procedure.

Our key objective is to compare phasing between numerical and PN waveforms. We can make a stronger connection to the underlying physics while avoiding issues with time alignment by comparing phases as a function of polarization frequency, which corresponds to twice the orbital frequency in the PN case. For circular inspiral this frequency should grow monotonically in time, with the frequency ω_c providing a physical reference of the "hardness" of the tightening binary.

Circular inspiral phasing information is typically derived in PN theory by imposing an energy balance relation to deduce the rate at which ω_c evolves from the radiation rate at a specified value of ω_c [1]. Though not strictly derived in the PN context, this physically sensible condition currently allows the determination of the *chirp rate* $\dot{\omega}_c(\omega_c)$ up to 3.5PN order [11]. From such a relation, information about phase and time are determined by integrating $d\phi/d\omega_c = \omega_c/\dot{\omega}_c$ and $dt/d\omega_c = 1/\dot{\omega}_c$. The phasing information can be represented by any one of several relations among phase, frequency, and time. Various approaches take the PN-expanded representation of one of these relations as the PN "result" for waveform phasing [1,11,18]. It has been demonstrated [11] that the PN expansion of $\dot{\omega}_c(\omega_c)$, numerically integrated as needed, has the greatest utility for conducting comparisons of phasing with numerical results during the late inspiral, and we adopt that convention.

For the purpose of comparison with our numerical simulations, we invert the monotonic function $\omega_c(t)$ to obtain

the phase as a function of frequency: $\phi(\omega_c) = \phi[t(\omega_c)]$. Note that the effect of eccentricity is not removed from ϕ, though the "circularized" frequency ω_c does provide the abscissa according to which phases are compared in the different treatments.

Figure 2 shows the wave phases as a function of $\omega_c M$; here each phase is adjusted by addition of a constant so that it vanishes at $\omega_c M = 0.054$, corresponding to the time $1000M$ before the radiation merger peak in the high-resolution numerical simulation. As demonstrated in Fig. 3, the sequence of numerical results converges at fourth order, allowing us to obtain a fifth-order-accurate result by Richardson extrapolation (thick solid line in Fig. 2).

In Fig. 2 we compare the numerical simulation results for the phase with the numerically integrated PN expansion of the chirp rate at 2.5PN, 3PN, and 3.5PN order. The agreement of the extrapolated numerical result with the integrated PN chirp rate improves with each successive order, with the 3.5PN result showing striking agreement up to about $\omega_c M \sim 0.15$.

We look more quantitatively at this agreement in Fig. 3 by plotting the phase differences $\delta\phi$ that accumulate between different phase approximations, as a function of frequency. The thick dash-dotted curve shows the phase differences between our medium- and high-resolution results, while the thin dash-dotted curve shows the differences between our low- and medium-resolution results, scaled so that for fourth-order convergence the curves should superpose. This is indeed observed to good approximation. A good estimate for the error of the phase in the high-resolution run is given by its difference from the phase obtained by Richardson extrapolation; this comes out to ~93% of the medium-high curve shown in the figure. Note that the cumulative errors in the numerically generated waveforms accrue primarily at lower frequencies, scaling approximately as ω_c^{-5}; the thin dashed curve shows a fit to the medium-high curve with this scaling. The deviations of the medium-high curve from this fit show the effect of eccentricity in our simulations. This accumulation of phase errors at lower frequencies makes sense generally since the simulations spend longer in that regime.

Without monotonic convergence between the 2PN, 2.5PN, and 3PN at the frequencies considered here, it is difficult to estimate errors in the PN phase. Nonetheless we tentatively take the difference between the integrated 3PN and 3.5PN chirp rates, shown by the dashed line in Fig. 3, as an upper bound on errors in a 3.5PN waveform. We also show (thin dotted line) the accumulated phase differences between the integrated 2.5PN and 3PN chirp rates to show the relative contribution of the preceding PN term.

The trend in the slope of these error curves indicates the rate at which phase error accumulates, as independently estimated within each approach. The slope of the fit to the medium-high error curve in Fig. 3 is initially higher than that of the 3PN–3.5PN error curve, but decreases steadily, matching the PN error-curve slope around $\omega_c M \sim 0.08$ and less thereafter. For clarity a piece of the 3PN–3.5PN curve has been translated upward to fit to the medium-high curve in Fig. 3. This suggests that phasing errors for our high-resolution simulation accumulate more quickly than 3.5PN phasing errors for $\omega_c M \lesssim 0.08$ ($t \lesssim -300M$), with the numerical simulation phasing being more accurate than PN at higher frequencies. In both cases, the phase error accumulates to roughly two radians by $\omega_c M \sim 0.15$ as the black holes begin to plunge together.

We now address the central objective of this Letter, a quantitative comparison of numerical and PN phasing

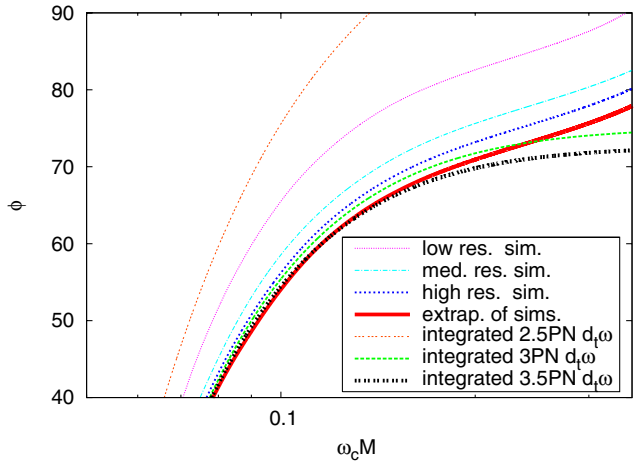

FIG. 2 (color online). Gravitational-wave phase, in radians, for numerical and PN waveforms. The solid curve is a Richardson extrapolation of the numerical results. The solid curve agrees well with the phase obtained by numerically integrating the 3.5PN expansion of the chirp rate $\dot{\omega}_c(\omega_c)$. Each successive PN order shown agrees better with the Richardson-extrapolated result, although this is not true of all the preceding terms in the PN sequence, since the sequence does not converge monotonically.

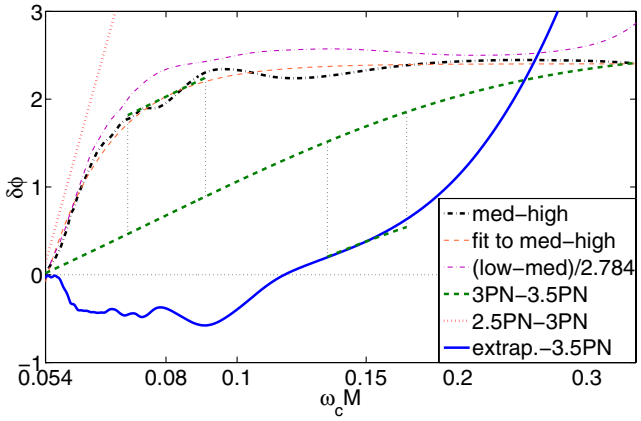

FIG. 3 (color online). Gravitational-wave phase-error estimates. Differences between phasing from the integrated 3.5PN chirp rate and Richardson extrapolation from the numerical simulations (solid curve) are small, and are consistent with internal error estimates for the numerical simulation results and the PN sequence. Curves which involve numerical phases are smoothed to remove high frequency noise.

results. We compare the Richardson-extrapolated phase, our best simulation estimate, with the integrated 3.5PN chirp-rate result. The difference is shown in the solid curve of Fig. 3. Note that, overall, the phase differences between the PN and numerical results (solid curve) accumulate less rapidly than the estimated errors in either the high-resolution simulation or the 3.5PN results over much of the frequency range shown. This illustrates that the numerical and post-Newtonian predictions appear to be converging to a common answer for waveform phase, in a frequency regime where the validity of the PN predictions could not previously be assessed. In the range $0.1 \lesssim \omega_c \lesssim 0.15$ the slope of the trend in the solid curve surpasses that of the 3PN–3.5PN curve, with the precise crossover point obscured by the effect of eccentric oscillations in the numerical simulations; we have translated a portion of the 3PN–3.5PN curve down to the solid line for clarity. After this range, corresponding to $-170 \lesssim t/M \lesssim -70$, and occurring 1 to 3 wave cycles before the estimated end of the binary's last orbit, the phase difference between the best estimates of the numerical and PN approaches grows more significantly.

Through the frequency range $0.054 \lesssim \omega_c M \lesssim 0.15$ the net phase difference, measured against frequency, amounts to less than 1 rad, a level of error that would be tolerable in many gravitational-wave data analysis applications. Superficially, phase differences in Fig. 1 may appear smaller than the differences quantified in Fig. 3. This is because the differences in chirp rate are more directly evident in the frequency-based phase comparisons. This more immediate connection to the merger dynamics, together with the avoidance of time-alignment issues, makes frequency-based phase comparisons a more reliable indicator of phasing differences.

Our results provide a crucial cross-validation of PN waveforms from the late inspiral of binary merger, with results of new long-lasting numerical simulations. These simulations have sufficient accuracy to provide a meaningful comparison with PN waveforms over the last $t \sim 1000M$ of the coalescence, specifically addressing a binary system of equal-mass nonspinning black holes. We find phase agreement consistent with internal phase-error estimates conducted in each approach, indicating that phase accuracies within a few radians are now achievable for this part of the coalescence waveform.

We emphasize, however, that there is still much important work to be done in improving and further assessing PN and numerical simulation waveforms. Certainly we have only addressed one case in a large parameter space of potential binaries, which will inevitably include systems, such as rapidly precessing unequal-mass spinning binaries, that are harder to treat with present PN and numerical techniques. With either approach, even for our simple case, a non-negligible amount of phasing error accumulates over the range studied, and more will have accumulated at lower frequencies addressable through the PN approximation. We expect continuing developments in numerical simulations and the pursuit of higher-order PN treatments to be crucial for developing a refined understanding of coalescence waveforms, which will be crucial in some data analysis applications for gravitational-wave observations.

This work was supported in part by NASA Grant No. O5-BEFS-05-0044. The simulations were carried out using Project Columbia at NASA Ames Research Center. J. v. M. and B. K. were supported by the NASA Postdoctoral Program at the Oak Ridge Associated Universities.

[1] L. Blanchet, Living Rev. Relativity **9** (2006), http://relativity.livingreviews.org/Articles/lrr-2006-4/.
[2] A. Buonanno, Y. B. Chen, and M. Vallisneri, Phys. Rev. D **67**, 024016 (2003).
[3] F. Pretorius, Phys. Rev. Lett. **95**, 121101 (2005).
[4] M. Campanelli, C. O. Lousto, P. Marronetti, and Y. Zlochower, Phys. Rev. Lett. **96**, 111101 (2006).
[5] J. G. Baker, J. Centrella, D.-I. Choi, M. Koppitz, and J. van Meter, Phys. Rev. Lett. **96**, 111102 (2006).
[6] M. Campanelli, C. O. Lousto, and Y. Zlochower, Phys. Rev. D **73**, 061501(R) (2006).
[7] J. G. Baker, J. Centrella, D.-I. Choi, M. Koppitz, and J. van Meter, Phys. Rev. D **73**, 104002 (2006).
[8] M. Campanelli, C. O. Lousto, and Y. Zlochower, Phys. Rev. D **74**, 041501(R) (2006).
[9] M. Campanelli, C. O. Lousto, and Y. Zlochower, Phys. Rev. D **74**, 084023 (2006).
[10] J. A. Gonzalez, U. Sperhake, B. Brügmann, M. Hannam, and S. Husa, Phys. Rev. Lett. **98**, 091101 (2007).
[11] A. Buonanno, G. B. Cook, and F. Pretorius, Phys. Rev. D **75**, 124018 (2007).
[12] J. R. van Meter, J. G. Baker, M. Koppitz, and D.-I. Choi, Phys. Rev. D **73**, 124011 (2006).
[13] J. G. Baker, S. T. McWilliams, J. R.van Meter, J. Centrella, D.-I. Choi, B. J. Kelly, and M. Koppitz, Phys. Rev. D **75**, 124024 (2007).
[14] L. Blanchet, G. Faye, B. R. Iyer, and B. Joguet, Phys. Rev. D **65**, 061501 (2002); **71**, 129902(E) (2005).
[15] L. Blanchet, T. Damour, G. Esposito-Farese, and B. R. Iyer, Phys. Rev. Lett. **93**, 091101 (2004).
[16] K. G. Arun, L. Blanchet, B. R. Iyer, and M. S. S. Qusailah, Classical Quantum Gravity **21**, 3771 (2004); **22**, 3115(E) (2005).
[17] C. Cutler *et al.*, Phys. Rev. Lett. **70**, 2984 (1993).
[18] L. Blanchet, A. Buonanno, and G. Faye, Phys. Rev. D **74**, 104034 (2006); **75**, 049903(E) (2007).